ARTICLE

Electronic Supplementary Information

Received 00th January 20xx,
Accepted 00th January 20xx

DOI: 10.1039/x0xx00000x

Microwave-plasma induced one-step synthesis of $Ni(PO_3)_2$ nanospheres loaded bio-waste derived N, P co-doped carbon for the asymmetric supercapacitor with prolong life

Nisha Gupta, Pallab Bhattacharya*

Experimental Methods

Materials

Bio-waste coffee grounds were collected from NML canteen and local cafe, Phosphoric acid (H_3PO_4), Nickel nitrate hexahydrate $Ni(NO_3)_2.6H_2O$ and potassium hydroxide (KOH) as electrolyte were purchased from Merck Chemicals, India limited and used as received. Solvents like N-Methyl-2-Pyrrolidone (NMP) and ethanol are also purchased from Merck Chemicals, India.

Materials Characterizations

Crystallographic structure and phase information of all the developed samples were analysed by XRD Bruker, D8 DISCOVER semiautomatic diffractometer using Cu-Kα radiation (λ = 0.154178 nm) with a scan speed of 1˚C min^{-1} at wide-angle range of 2θ value 10 to 60˚ where accelerating voltage of 50 kV and the emission current of ~300 mA was used. The chemical diversities of different doped and undoped material were investigated through X-ray photoelectron spectrometer (SPECS, Germany) with an Mg-Kα twin anode X-ray source (E = 1253.6 eV). The binding energies were collected with a reference to the maximum intensity of the C1s (284.6 eV). Analysis of the spectra was done using CASA XPS software. Scanning electron microscopy was performed in a (Nova Nano SEM 430, Netherland make SEM) to analyze microstructures and morphologies. High resolution transmission electron microscopy was analysed with (HRTEM JEOL JEM-1230 with accelerating voltage of 120 kV). FTIR is used to determine the functional groups in the range of 500-4000 cm^{-1} where the sample was fabricated with KBr. Raman spectra of the synthesized powdered materials were recorded using a WITEC-alpha 300 R Confocal Raman imaging. Powdered materials were on the glass slide for spectra recoding using 532 nm laser source. BET surface area was determined by N_2 adsorption desorption method using Nova 4000e (Quantachrome, USA). Prior to adsorption desorption measurements, the samples were degassed at 473 K at 10^{-3} Torr for 5 h. Thermogravimetric analysis (TGA) analysis was carried out in a NETZSCH, STA 449 F5 Jupiter instrument in air atmosphere up to 900 ˚C at 10 ˚C min^{-1} to analyse the thermal stability of materials.

Electrode fabrication and electrochemical measurements

Electrochemical measurements were carried out both in three-electrode and two-electrode configuration by using a GAMRY workstation. Nickel foam has been used as a current collector for making the working electrodes. Graphite rod as a counter electrode, and Hg/Hg_2Cl_2 as a reference electrode has been used during three-electrode measurements. The working electrodes were prepared by mixing the suitable active material, conducting carbon black and PVDF embedded in NMP in a weight ratio of 80:10:10. Addition of adequate amount of NMP is required to make slurry of the above mixture which then coated on washed nickel foam and dried under vacuum oven at 60°C overnight to obtain the NPGC@1:1, NiPO, different ratios of NPGC-NiPO composites, and NPGC-NiPO-mix@1:1 working electrodes. The electrochemical studies were investigated using cyclic voltammetry (CV), galvanostatic charge-discharge (GCD), and electrochemical impedance spectroscopy (EIS), which were performed using GAMRY electrochemical work station. The electrochemical performances of the NPGC@1:1, NiPO, and different ratios of NPGC-NiPO@1:1:1 electrodes were evaluated in 6M KOH electrolyte in three-electrode cells. In the three-electrode system, gravimetric capacitance C_g (Fg^{-1}), of the electrode through GCD is calculated by the following equation:[1,2]

$$C_g = \frac{I \times \Delta t}{m \times \Delta V} \quad \ldots\ldots\ldots\ldots\ldots\ldots\ldots (1)$$

Where *I* is current (in A), *Δt* is discharge time (in s), *m* is mass (in g), and ΔV is potential window (in V), respectively.

The all-solid-state asymmetric supercapacitor devices are then fabricated by using NPGC-NiPO@1:1 as positive electrode and NPGC@1:1 as negative electrode, which is denoted as NPGC-NiPO@1:1:1//NPGC@1:1. To assure the optimized electrochemical performance of the NPGC-NiPO@1:1:1//NPGC@1:1 device, mass of both the electrode needs to be determined suitably by following the equation

$$\frac{m^+}{m^-} = \frac{C^- \times \Delta V}{C^+ \times \Delta V} \quad \ldots\ldots\ldots\ldots\ldots\ldots\ldots (2)$$

[a] *Functional Materials Group, Advanced Materials & Processes (AMP) Division, CSIR-National Metallurgical Laboratory (NML), Burmamines, East Singhbhum, Jamshedpur, Jharkhand-831007, India. E-mail: pallab.b@nmlindia.org.*

Electronic Supplementary Information (ESI) available: See DOI: 10.1039/x0xx00000x

Where m^+ is mass of positive electrode (in g), m^- is mass of negative electrode (in gram), C^+ is the capacitance of positive electrode (in Fg^{-1}), C^- is the capacitance of negative electrode (in Fg^{-1}), ΔV is potential window (in V), respectively. According to the charge balance calculation the appropriate mass ratio of NPGC@1:1 and NPGC-NiPO@1:1:1 will be 1:0.94 which has been followed for making the all-solid-state asymmetric supercapacitor devices.

To prepare the all-solid-state devices, PVA-KOH solid electrolyte needs to be prepared, and this has been made as 1 g of polyvinyl alcohol (PVA) powder was slowly added to dissolve into 10 mL of distilled water, and then the mixture was heated at 90°C under continuous stirring until the solution became clear. Then, 5 mL aqueous KOH (6M) was added dropwise slowly into the prepared PVA solution under constant stirring to get the required solid electrolyte. To keep the thickness of the separator constant, we always used 1 ml of the as-prepared PVA-KOH gel for a particular area of electrode. After that the solid electrolyte has been placed in between the positive and negative electrodes and dried properly to complete the process of making all-solid-state asymmetric supercapacitor devices.

The Trasatti method has been used to differentiate the contribution of EDLC and pseudocapacitance out of the total obtained capacitance of any electrodes, and it is a very common practice for various hybrid electrodes.[1] In this method, firstly, we obtained the CVs of NPGC@1:1, NiPO, and NPGC-NiPO@1:1:1 at different slow scan rates and then corresponding gravimetric capacitances has been calculated based on the following equation:[2-4]

$$C = \frac{S}{2 \times m \times \vartheta \times \Delta V} \quad \text{..... (3)}$$

where C stands for the gravimetric capacitance (in Fg^{-1}), ΔV the potential window (in V), m is the mass of the electrode, S the area enclosed by corresponding cyclic voltammograms (in AVg^{-1}) and ϑ the scan rate (in Vs^{-1}). Plotting the reciprocal of the gravimetric capacitances (C^{-1}) against the square root of scan rates ($\vartheta^{1/2}$) should yield a linear correlation between them, assuming semi-infinite diffusion of ions. Specifically, the correlation can be described by the following equation:

$$C^{-1} = Constant \times \vartheta^{1/2} + CT^{-1} \quad \text{.....(4)}$$

where C, ϑ and CT is the experimental gravimetric capacitance, the scan rate and the total capacitance, respectively. The "total capacitance" is equals the sum of EDL and pseudocapacitive. Plotting the gravimetric capacitances (C) against the reciprocal of square root of scan rates ($\vartheta^{1/2}$) also give a linear correlation described by the following equation:

$$C = Constant \times \vartheta^{1/2} + C_{EDL} \quad \text{..... (5)}$$

where C, ϑ and C_{EDL} is the experimental gravimetric capacitance, the scan rate and the EDLC, respectively. Linear fit the plot and extrapolate the fitting line to y-axis gives the maximum EDL. Subtraction of C_{EDL} from CT yields the maximum pseudocapacitance. Finally, the capacitance contribution percentage from EDL capacitance and pseudocapacitance can be calculated by following equation:

$$C_{EDL\,\%} = \frac{C_{EDL} \times 100}{C_T} \quad \text{..... (6)}$$

Calculation of carbon yield%

$$Yield\,\% = \frac{W_C \times 100}{W_O} \quad \text{..... (7)}$$

Where W_c is the dry weight (g) of final activated carbon and Wo is the dry weight (g) of biowaste.

Supplementary Figures

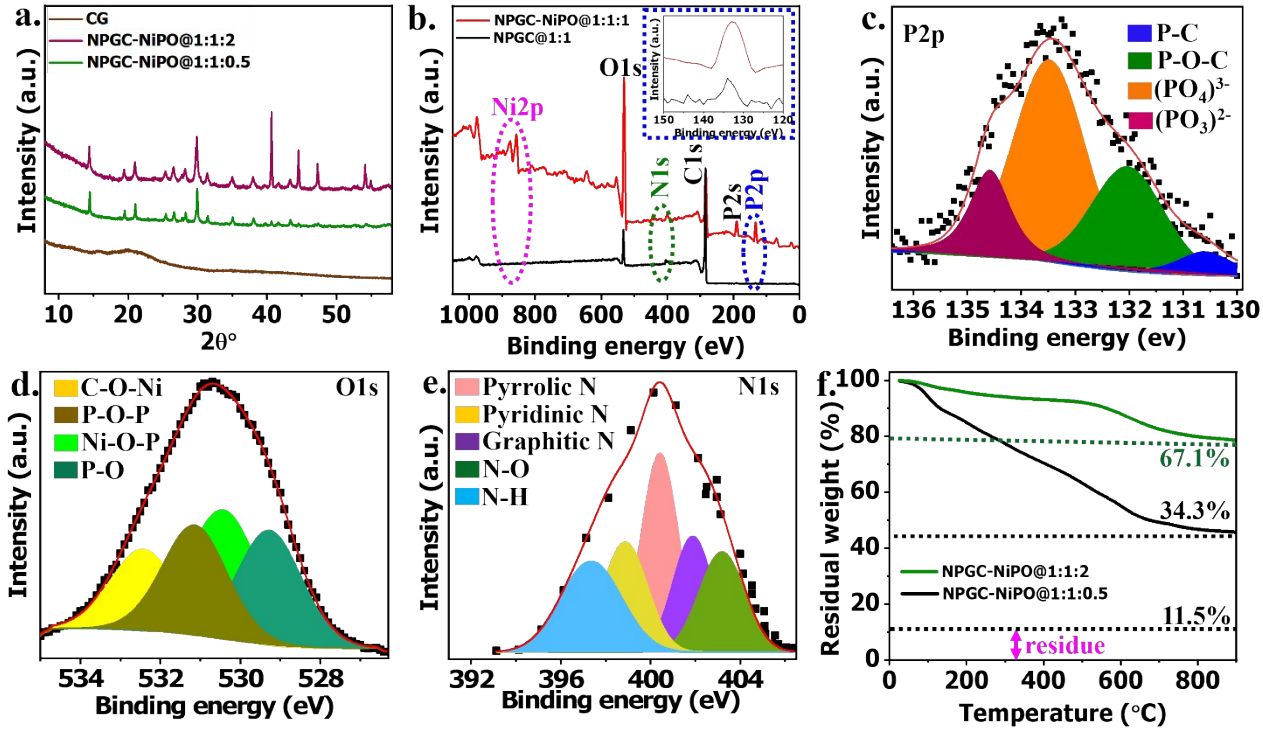

Figure S1. (a) XRD of CB, NPGC-NiPO@1:1:0.5 and NPGC-NiPO@1:1:2; XPS survey analysis of (b) NPGC@1:1 and NPGC-NiPO@1:1:1 (Inset shows the magnified P2p peak); fitted high resolution XPS plot of (c) P2p XPS plot of NPGC@1:1, (d) O1s and (e) N1s XPS plot of NPGC-NiPO@1:1:1; (f) TGA spectra of NPGC-NiPO@1:1:0.5 and NPGC-NiPO@1:1:2.

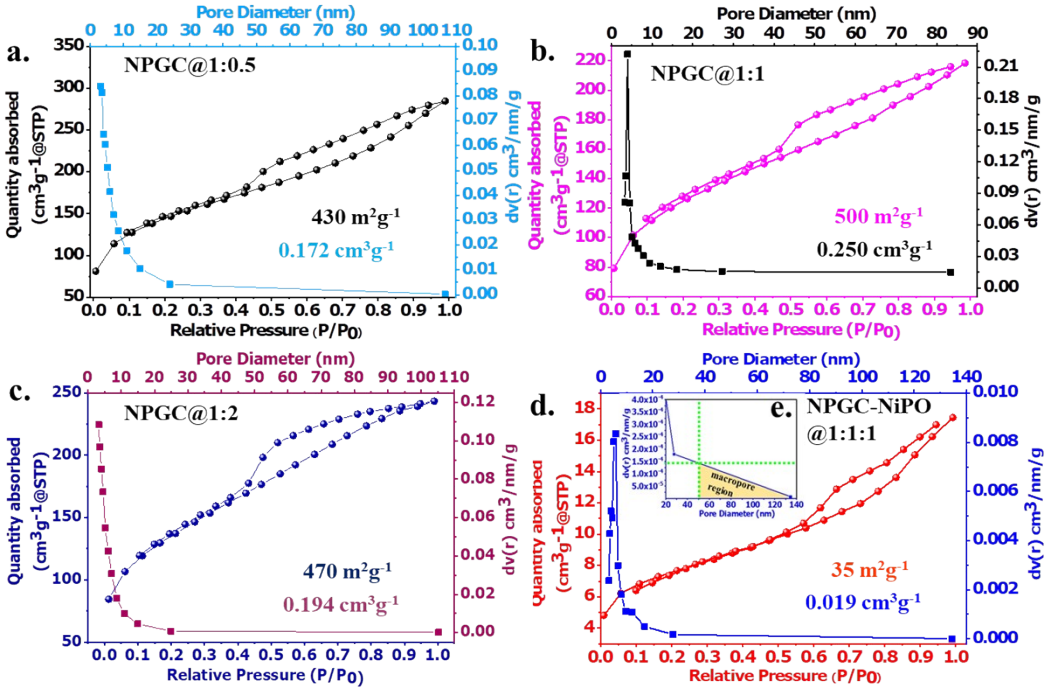

Figure S2. Isotherm and pore diameter plot of (a) NPGC@1:0.5, (b) NPGC@1:1, (c) NPGC@1:2, (d) NPGC-NiPO@1:1:1, and (e) inset shows the magnified BJH plot of NPGC-NiPO@1:1:1

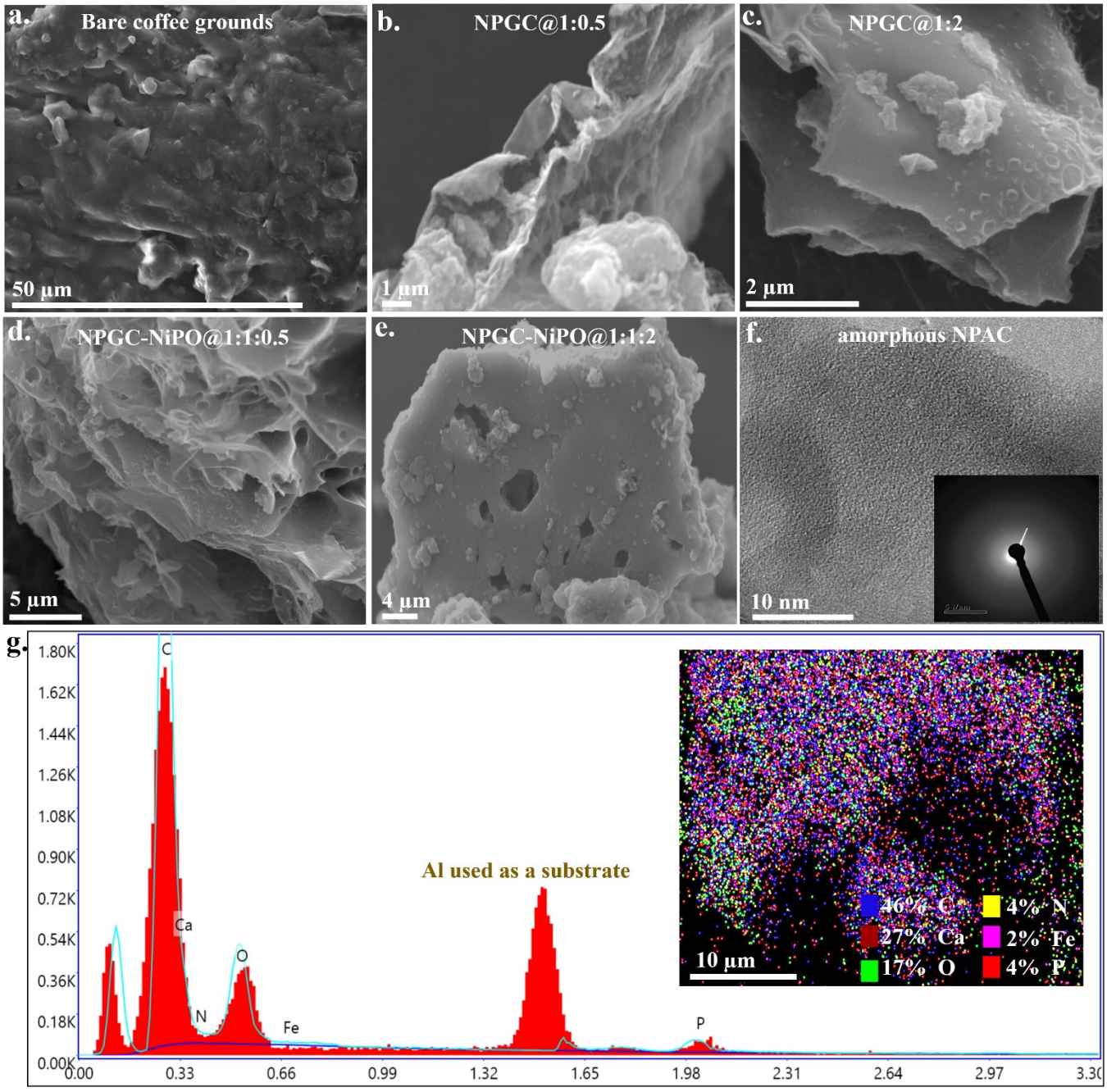

Figure S3. SEM image of (a) bare coffee grounds, (b) NPGC@1:0.5, (c) NPGC@1:2, (d) NPGC-NiPO@1:1:0.5, and (e) NPGC-NiPO@1:1:2; (f) TEM image of amorphous NPAC (inset SAED pattern of NPAC), (g) EDS plot with colour mapping of the residue obtained after TGA of NPGC@1:1.

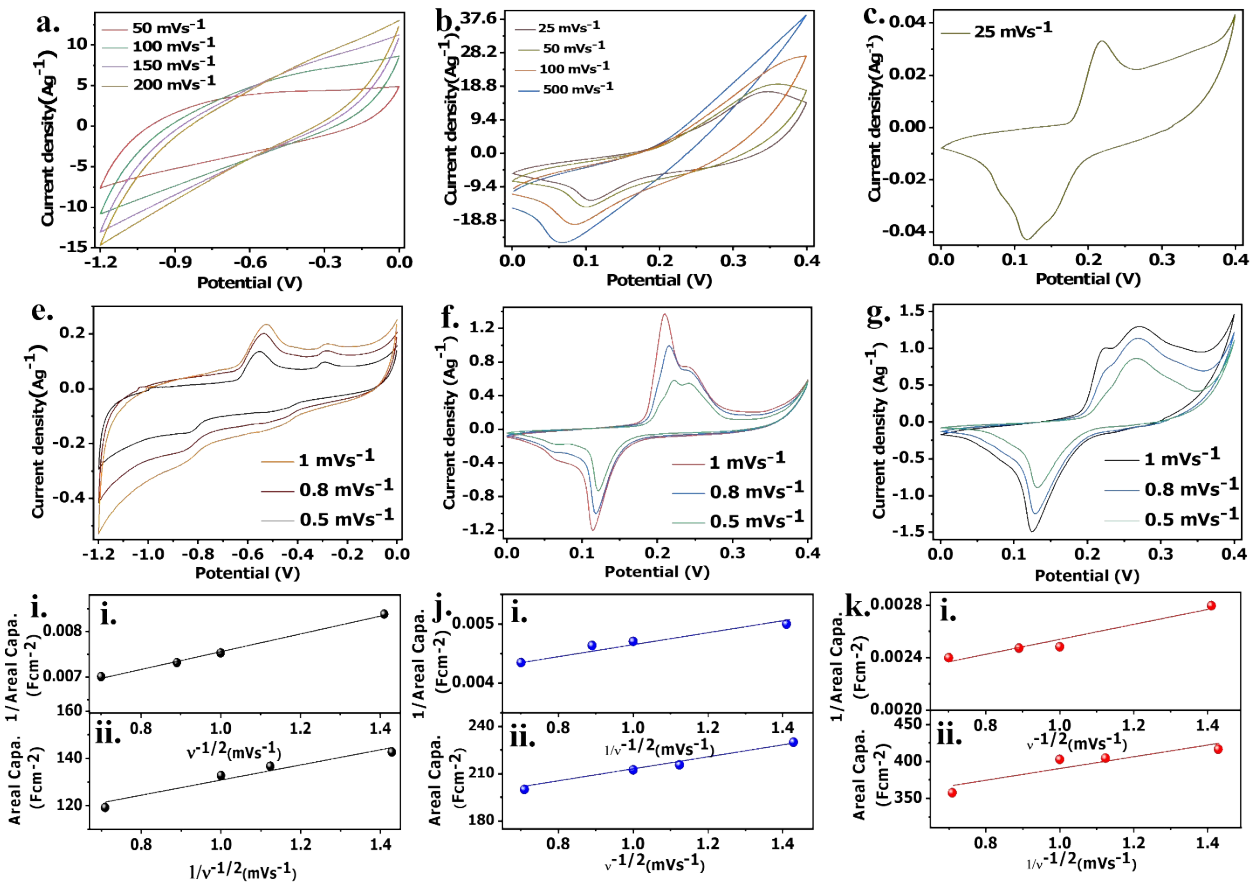

Figure S4. CV analysis of (a) NPGC@1:1, (b) NPGC-NiPO@1:1:1 at different scan rates, (c) bare Ni foam, (d) NPGC@1:1, (e) bare NiPO, and (f) NPGC-NiPO@1:1 at low scan rates; Trasatti's method for (i) NPGC@1:1, (j) NiPO, and (k) NPGC-NiPO@1:1:1 at (i) inverse capacitance as a function of square root of scan rate; (ii) capacitance as a function of inverse square root of scan rate.

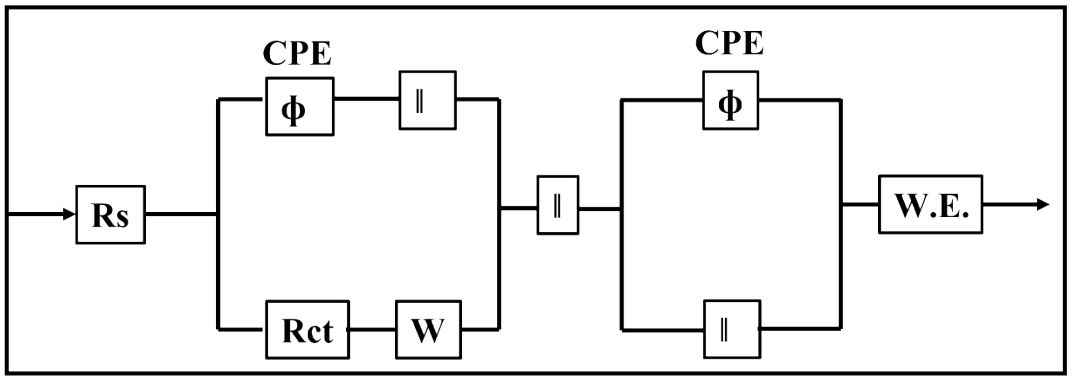

Figure S5. EIS circuit model used in Nyquist plot fitting.

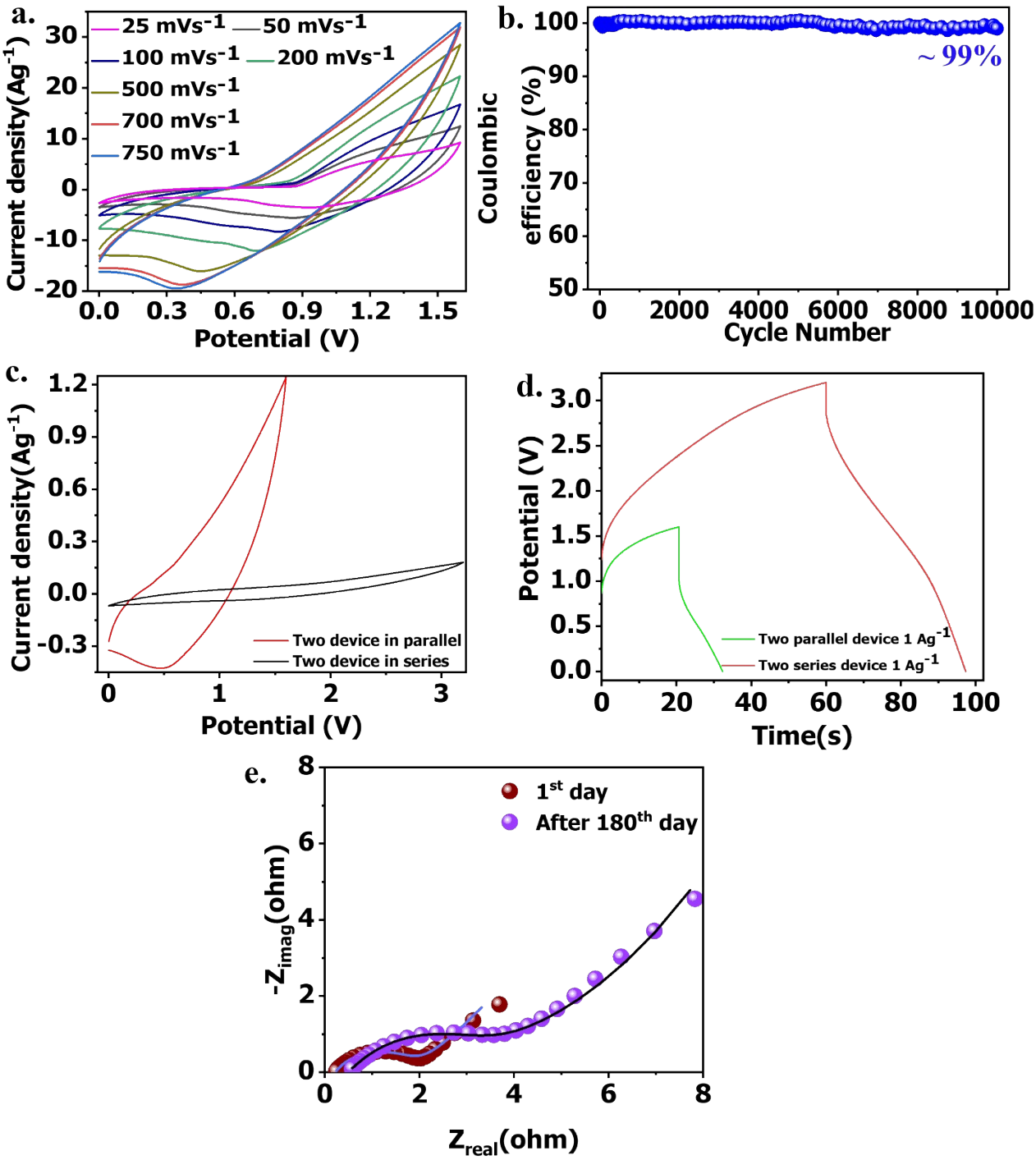

Figure S6. CV analysis of (a) NPGC@1:1//NPGC-NiPO@1:1:1 single device at higher scan rate, (b) Coulombic efficiency plot of NPGC@1:1//NPGC-NiPO@1:1:1, (c) NPGC@1:1//NPGC-NiPO@1:1:1 two device in series, and NPGC@1:1//NPGC-NiPO@1:1:1 two device in parallel; GCD of (d) NPGC@1:1//NPGC-NiPO@1:1:1 two device in series and parallel; (e) Nyquist plot of NPGC@1:1//NPGC-NiPO@1:1:1 two device in series in 1st day and after 180th day.

Supplementary Tables

Table S1: Comparison of yield percentages of carbon derived from different biomasses

Biowaste	Processing condition	Carbon yield	Ref.
Jatropha hull	Microwave	16.6 %	5
Bovine blood waste	Microwave	2 %	6
Feedstock	Microwave	28 %	7
Core	Calcination	27.8 %	8
Shaggy	Calcination	28.57 %	8
Oil palm empty fruit bunch	Calcination	19.3 - 27.9%	9
Olive stones	Calcination	31 %	10
NPGC@1:1	Microwave	37.5 %	This work

Table S2: Comparison of energy storage performances of electrodes made of different carbon and transition metal phosphates based electrodes

Name of the electrodes	Processing conditions	Electrolyte	Capacitance@current density	Potential window	Retention performance	Reference
Electrode of bio-waste derived carbon-transition metal phosphates composite						
NPGC-NiPO@1:1:1	Microwave plasma induced single-step approach	6M KOH	417 Fg^{-1}@1 Ag^{-1} 300.6 $mFcm^{-2}$ @4.5 $mAcm^{-2}$	0.4 V	93 % after 10000 cycles	This work
No other reports are available						
Electrodes made of other than bio-waste derived carbon-transition metal phosphates composite						
$Mn_3(PO_4)_2$-Graphene foam (GF)	Multiple steps along with CVD process	6 M KOH	270 Fg^{-1}@0.5 Ag^{-1}	0.4 V	99 % after 1000 cycles	11
$Ni(NH_4)_2(PO_3)_4{\cdot}4H_2O$-GF	Multiple steps along with CVD process	6M KOH	52 $mAhg^{-1}$ @0.5 Ag^{-1}	0.5 V	98% after 5000 cycles	12
$NiCo(PO_4)_3$-GF	Multiple steps along with CVD process	1M KOH	86.4 $mAhg^{-1}$@1Ag^{-1}	0.45 V	Not reported	13
$Ni_2P_2O_7$	Hydrothermal	4M KOH	120 Fg^{-1}@2 Ag^{-1}			14
$Mn_3(PO_4)_2$		1M Na_2SO_4	203 Fg^{-1}@0.5 Ag^{-1}	1.6 V	88% after 10000 cycles	15
$NaNiPO_4$	Calcination	2M NaOH	125 Fg^{-1}@1 Ag^{-1}	0.6 V	99% after 2000 cycles	16
Elaeocarpus tectorius	Calcination	1M H_2SO_4	201 Fg^{-1}@1 Ag^{-1}	1 V	71% after 2000 cycles	17
Fir sawdust	One-step carbonization	1M H_2SO_4	169 Fg^{-1}@0.5 Ag^{-1}	0.8 V	98.3% after 5000 cycles	18

Reference

1. S. Ratha, S. Sahoo, P. Mane, B. Polai, B. Sathpathy, B. Chakraborty, & S. K. Nayak, Experimental and computational investigation on the charge storage performance of a novel Al_2O_3-reduced graphene oxide hybrid electrode. *Scientific Reports.*, 2023, **13**, 5283.

2. B.H. Hameed, I.A.W. Tan, A.L. Ahmad, Preparation of oil palm empty fruit bunch-based activated carbon for removal of 2,4,6-trichlorophenol: Optimization using response surface methodology, *J. Hazardous Mater.*, 2009, **164,** 1316-1324.

3. M.Z. Alam, E. S. Amee m, S.A. Mu yibi, N.A. Kabba shi, The factors affecting the performance of activated car bon prepared from oil palm empty fruit bunches for adsorption of phenol, *Chem. Eng. J.*, 2009, **155**, 191-198

4. S.M., Yakout, and G.S. El-Deen, Characterization of activated carbon prepared by phosphoric acid activation of olive stones. *Arabian journal of chem.*, 2016, **9**, S1155-S1162.

5. D. Xin-hui, C. Srinivasakannan, P. Jin-hui, Z. Li-bo, Z. Zheng-yong, Comparison of activated carbon prepared from Jatropha hull by conventional heating and microwave heating. *Biomass and Bioenergy*. 2011, **35**, 3920–3926.

6. N. Chalmpes, G. Asimakopoulos, M. Baikousi, D. Moschovas, A. Avgeropoulos, A. B. Bourlinos, V. Sedajova, A. Bakandritsos, D. Gournis, & M. A. Karakassides, Fast and direct microwave synthesis of carbon from bovine blood waste: a feedstock material for extractive metallurgy, carbon dots production and graphite synthesis. *J. Nanotechnol. Res.*, 2021, **3**, 011-028.

7. J. Czarnocka, The use of microwave pyrolysis for biomass processing, *Archiwum Motoryzacji*, 2015, **67**, 11-21.

8. N. B. Osman, N. Shamsuddin, & Y. Uemura, Activated carbon of oil palm empty fruit bunch (EFB); core and shaggy, *Procedia eng.*, 2016, **148**, 758-764.

9. M.Z. Alam, E. S. Amee m, S.A. Mu yibi, N. A. Kabba shi, The factors affecting the performance of activated carbon prepared from oil palm empty fruit bunches for adsorption of phenol, *Chem. Eng. J.*, 2009, **155**, 191-198.

10. S. M. Yakout, & G. S. El-Deen, Characterization of activated carbon prepared by phosphoric acid activation of olive stones, *Arabian journal of chem.*, 2016, **9**, S1155-S1162.

11. A. A. Mirghni, M. J. Madito, T. M. Masikhwa, K. O. Oyedotun, A. Bello, N. Manyala, Hydrothermal synthesis of manganese phosphate/graphene foam composite for electrochemical supercapacitor applications, *J Colloid Interface Sci.*, 2017, **494**, 325-337.

12. B. A. Mahmoud, A. A. Mirghni, O. Fasakin, K. O. Oyedotun, & N. Manyala, Bullet-like microstructured nickel ammonium phosphate/graphene foam composite as positive electrode for asymmetric supercapacitors. *RSC Adv.*, 2020, **10**, 16349-16360.

13. A. A. Mirghni, K. O. Oyedotun, B. A. Mahmoud, A. Bello, S. C. Ray, & N. Manyala, Nickel-cobalt phosphate/graphene foam as enhanced electrode for hybrid supercapacitor, *Composites Part B: Eng.*, 2019, **174**, 106953.

14. M. Priyadharshini, M. Sandhiya, M. Sathish, T. Pazhanivel, Surfactant-dependant self organisation of nickel pyrophosphate for electrochemical supercapacitors, *J. Mater. Sci. Mater. Electron.*, (2021),

15. X.J. Ma, W.B. Zhang, L.B. Kong, Y.C. Luo, L. Kang, Electrochemical performance in alkaline and neutral electrolytes of a manganese phosphate material possessing a broad potential window, *RSC Adv.*, 2016, **6**, 40077–40085

16. M. Minakshi , D. Mitchell , R. Jones , F. Alenazey , T. Watcharatharapong , S. Chakraborty and R. Ahuja , *Nanoscale.*, 2016, **8** , 11291 -11305

17. B. Nirosha, R. Selvakumar, J. Jeyanthi and S. Vairam, Elaeocarpus tectorius derived phosphorus-doped carbon as an electrode material for an asymmetric supercapacitor.zzzz *New J. Chem.*, 2020, **44**, 181–193.

18. G. Lin, Q. Wang, X. Yang, Z. Cai, Y. Xiong, & B. Huang, Preparation of phosphorus-doped porous carbon for high performance supercapacitors by one-step carbonization. *RSC adv.*, 2020, **10**, 17768-17776.